Photoacoustics 37 (2024) 100598

Contents lists available at ScienceDirect

Photoacoustics

journal homepage: www.elsevier.com/locate/pacs

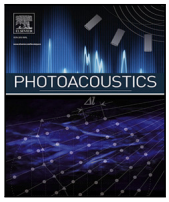

Research article

A multi-aperture encoding scheme for increased SNR in photoacoustic Imaging

Amir Gholampour [a,*], Camilo Cano [a], Marc R.H.M. van Sambeek [a,b], Richard Lopata [a], Min Wu [a], Hans-Martin Schwab [a]

[a] Photoacoustics and Ultrasound Laboratory Eindhoven (PULS/e), Department of Biomedical Engineering, Eindhoven University of Technology, Eindhoven, 5600 MB, The Netherlands

[b] Department of Vascular Surgery, Catharina Hospital Eindhoven, Eindhoven, 5602 ZA, The Netherlands

ARTICLE INFO

Keywords:
Encoding
CMUT
Multi-aperture
Coherent compounding
Photoacoustic imaging
SNR

ABSTRACT

Photoacoustic imaging creates light-induced ultrasonic signals to provide valuable information on internal body structures and tissue morphology non-invasively. A multi-aperture photoacoustic imaging (MP-PAI) system is an improvement over conventional photoacoustic imaging (PAI) systems in terms of resolution, contrast, and field of view. Previously, a prototype MP-PAI system was introduced based on multiple capacitive micromachined ultrasound transducers (CMUTs) with shared channels, such that each element in a CMUT shares its channel with its counterpart in other CMUTs. The system uses the biasing voltages of the CMUTs to switch between them and multiplex the received signals in time. Notwithstanding all the enhancements, the signal-to-noise ratio (SNR) remains limited in PAI. To address this issue, we are proposing a multi-aperture encoding scheme (MAES) to further increase the SNR in a multi-aperture PAI system. The proposed method involves receiving signals with multiple CMUTs simultaneously based on an encoding matrix, instead of switching between individual CMUTs. As a result, shared channels contain a superposition of signals, which are later recovered by applying a decoding matrix. Here, an analytical model for computing SNR with an arbitrary encoding sequence is presented, and the method is validated through numerical simulations and in an experimental study. Bipolar and unipolar encoding sequences were considered for the experiments. The numerical results show, in comparison to conventional MP-PAI, that MAES will obtain an SNR gain of 5.8 and 8.8 dB for S-sequence and truncated Hadamard encodings, respectively, when using 15 transducers. In experiments, three transducers are encoded by S-sequences and show 1.5 dB improvement in SNR over conventional MP-PAI method, which aligns well with the analytical model.

1. Introduction

Photoacoustic imaging is a promising biomedical imaging technique that can visualize different tissue constitutes [1–3]. However, signal-to-noise ratio (SNR), resolution, and field of view (FOV) are limited in photoacoustic imaging (PAI) [4]. It has been shown previously that extra apertures can be employed in a PAI system to increase the effective sensor area and subsequently improve the resolution and FOV [5–7]. An MP-PAI system can greatly benefit from capacitive micromachined ultrasonic transducers (CMUTs) as they are low-cost, versatile in design, and, more importantly, can offer a higher bandwidth compared to piezoelectric transducers [8–11]. Nonetheless, an imaging system with multiple transducers requires an increased number of channels, which is not practical for a large number of transducer elements. Multiplexing the received signals in time could be a solution [12,13]. we have previously proposed a simple approach [7] for multiplexing multiple CMUTs in time by sharing the communication channels among all the CMUTs, i.e., one element in each aperture shares the channel with an element of all other apertures. Then, the MP-PAI is performed by alternating the CMUTs using their biasing voltages [7]. However, time multiplexing will increases the acquisition time and reduce the imaging frame rate, which can be especially problematic for low-SNR PAI systems as it usually requires averaging between frames to reach a satisfactory SNR [14]. Thus, to increase SNR without highly reducing frame rate, we propose an aperture encoding technique. For both ultrasound and photoacoustic imaging, encoding methods have been investigated in the past. For example, encoding has been used in synthetic transmit aperture ultrasound systems to increase the SNR or frame rate via Hadamard sequences [15,16]. In this approach, multiple elements are excited using encoded waveforms; subsequently, a decoding step

* Corresponding author.
E-mail address: a.gholampour@tue.nl (A. Gholampour).

https://doi.org/10.1016/j.pacs.2024.100598
Received 20 November 2023; Received in revised form 1 February 2024; Accepted 20 February 2024
Available online 23 February 2024

yields the response for each element of the transducer. Ceroici et al. proposed an encoding of a 2D crossed-electrode relaxor array for PAI system using Hadamard patterns to receive signals across all elements while maintaining the channel counts, resulting in an increased SNR compared to a single-column biasing strategy [17].

However, in photoacoustics, the implementation of bipolar codes such as Hadamard sequences in practical applications is challenging, since it may require advanced electronics, e.g., signal inverters, or necessitate extra imaging sessions. These factors will increase the complexity and cost of the system, and in some cases, the use of bipolar codes may not be feasible [18–22]. Therefore, a unipolar variant of Hadamard sequences, so-called S-sequences, has been introduced as an alternative. Barber et al. used S-sequence encoding in a synthetic aperture photoacoustic computed tomography system which led to a significant increase in SNR compared to the conventional synthetic aperture method [23]. Hahamovich et al. introduced an physical acoustic mask using S-sequences to spatially encode a 2D aperture yielding an improved FOV, resolution, and SNR for 3D photoacoustic imaging [24]. Beckmann et al. proposed encoding and transmitting multiple-wavelength pulses in multispectral laser diode systems to simultaneously improve SNR and retain spectral information [25].

In this work, we investigate encoding strategies for complete apertures in a multi-aperture imaging scheme. Based on our prior work on a multiplexed multi-aperture PAI system for carotid plaque imaging [7], in this study, we propose a novel spatial encoding technique for signal acquisition. This approach aims to increase the SNR without further sacrificing the imaging frame rate compared to multiplexed MP-PAI. In conventional MP-PAI, each imaging session utilizes a single aperture to receive signals, generating a single-perspective image; these images are then acquired for all different apertures, and compounded to create the final MP-PAI image. Here, each imaging session utilizes a single aperture to receive signals, generating a single-perspective image; these images are then acquired for all different apertures, and compounded to create the final MP-PAI image. Here, we propose to use multiple apertures simultaneously in an encoded sequence, such that the superposition of the received signals from different apertures will be recorded. The signals from individual apertures are thereafter recovered by a decoding step prior to the image reconstruction.

A theoretical analysis of the expected SNR for a multi-aperture encoding scheme (MAES) is presented. The method is validated using both numerical and experimental studies. In simulations, MAES is evaluated in terms of SNR for an increasing number of apertures. Finally, the proposed method was implemented using a multi-aperture array consisting of three CMUTs, designed to image carotid plaques [7].

2. Methods

2.1. Encoding scheme theory

A theoretical framework is provided to analyze noise levels in a multi-aperture imaging setup. In the following derivation, we are assuming an additive, independent noise regime, where the noise $\boldsymbol{n}$ consists of identically distributed random values that follow a normal distribution with a zero mean and standard deviation of $\sigma_{\boldsymbol{n}}$. For band-pass signals, as in PAI, if the signal variance is assumed to be $Var(\boldsymbol{x}) = \sigma_{\boldsymbol{x}}^2$, we can conventionally define the SNR as:

$$\mathrm{SNR}_{\mathrm{conv}} = \frac{Var(\boldsymbol{x})}{Var(\boldsymbol{n})} = \frac{\sigma_{\boldsymbol{x}}^2}{\sigma_{\boldsymbol{n}}^2}. \tag{1}$$

A common approach to increase the SNR in PAI is the coherent averaging of received signals across multiple frames [14,26,27], where each frame is formed by multiple imaging sessions, i.e., reception of multiple light-induced photoacoustic signals. A similar result is obtained by reconstructing each imaging session and simply average them before the envelope detection, forming a coherently compounded image [7]. Assuming two random variables with distribution $\boldsymbol{g}$ and $\boldsymbol{h}$, the variance can be calculated with $Var(\boldsymbol{g}+\boldsymbol{h}) = Var(\boldsymbol{g}) + Var(\boldsymbol{h}) + Cov(\boldsymbol{g},\boldsymbol{h})$ in which $Cov(\boldsymbol{g},\boldsymbol{h}) = 0$ for independent random variables. Therefore, in summation of M frames coherently, the noise will still be Gaussian with a variance of $M\sigma_{\boldsymbol{n}}^2$ and zero mean. If the target signals are in complete correlation, the variance of M correlated signals will be $M^2\sigma_{\boldsymbol{x}}^2$, so the SNR is calculated as:

$$\mathrm{SNR}_{\mathrm{coh}} = \frac{M\sigma_{\boldsymbol{x}}^2}{\sigma_{\boldsymbol{n}}^2} \tag{2}$$

yielding a linear SNR gain with a factor of M when compared to a single frame PAI (Eq. (1)). From now on, We refer to the $\mathrm{SNR}_{\mathrm{coh}}$ as conventional multi-perspective photoacoustic imaging (MP-PAI) SNR.

An encoding scheme can be employed in M imaging sessions where the vector $\boldsymbol{x}$ is measured via a linear projection of the signals through a multiplicative weighing matrix $\mathbf{W}$. Fig. 1 shows the process of MAES imaging in which the superimposed signals are recorded and decoded to obtain an image with increased SNR. The weight matrix $\mathbf{W}$, defined as $\mathbf{W} = [w_{ij}]$, is an $M \times M$ matrix, where each row specifies the coding sequence for the apertures in each imaging session, with entries that do not exceed one, i.e. $\forall w_{ij} \in \mathbf{W}, 0 \le w_{ij} \le 1$. The imaging process can be mathematically described by:

$$\boldsymbol{y} = \mathbf{W}\boldsymbol{x} + \boldsymbol{n} \tag{3}$$

where $\boldsymbol{y}$ is the measurements vector at each instance of time t, with each row containing the measurements of one imaging session, and $\boldsymbol{n}$ is the noise vector at t describing the electrical–thermal disturbances in the circuitry. In other words, $y_1 = \sum_{m=1}^{M} w_{1m}x_m + n_1$ represents a snapshot of the measured signal at a specific time point from the first session of imaging and so forth, where w_{1m} denotes the first row and mth column of the matrix $\mathbf{W}$. Assuming $\mathbf{W}$ is orthogonal and has an inverse equal to $\mathbf{Z} = \mathbf{W}^{-1}$, the acoustic signals are recovered from the measurement via $\tilde{\boldsymbol{x}} = \mathbf{Z}\boldsymbol{y}$, resulting in

$$\tilde{\boldsymbol{x}} = \boldsymbol{x} + \boldsymbol{Z}\boldsymbol{n}. \tag{4}$$

The variance for the noise in the resulting measurement is given by $Var(\mathbf{Z}\boldsymbol{n})$ which can be expanded to $E\{(\mathbf{Z}\boldsymbol{n})^2\} - E\{\mathbf{Z}\boldsymbol{n}\}^2$ where the latter component is equal to zero as defined. The variance of the noise for a single aperture m in different sessions of i and j is described by:

$$E\{(\mathbf{Z}\boldsymbol{n})^2\} = E\{\sum_i (z_{mi})^2 n_i^2 + \sum_i \sum_{j\neq i} z_{mi}n_i z_{mj}n_j[1-\delta_{ij}]\} \tag{5}$$

where z_{mi} and z_{mj} represent the entries of the matrix $\mathbf{Z}$, corresponding to the mth row and the ith and jth columns, respectively. The last term in Eq. (5) is zero, given that the covariance of n_i and n_j is zero for $i \neq j$, as two instances of noise are uncorrelated. Hence, we get

$$E\{(\mathbf{Z}\boldsymbol{n})^2\} = \sigma_n^2 \sum_i (z_{mi})^2 \tag{6}$$

The general SNR for single transducer m using encoded multi-perspective imaging is as follows:

$$\begin{aligned}\mathrm{SNR}_{\mathrm{st}} &= \frac{Var(\boldsymbol{x})}{Var(\mathbf{Z}\boldsymbol{n})} \\ &= \frac{\sigma_x^2}{\sigma_n^2 \sum_i (z_{mi})^2}\end{aligned} \tag{7}$$

By coherently compounding M single perspective images to form the final reconstruction, similar to the calculation leading to Eq. (2), Eq. (7) can be written as:

$$\mathrm{SNR}_{\mathrm{enc}} = \frac{M\sigma_x^2}{\sigma_n^2 \sum_i (z_{mi})^2} \tag{8}$$

assuming complete coherency between received signals from different apertures. By Eq. (8) can be reformulated as:

$$\mathrm{SNR}_{\mathrm{enc}} = g\,\mathrm{SNR}_{\mathrm{coh}} \tag{9}$$

where the SNR gain over conventional MP-PAI is equal to $g = 1/\sum_i (z_{mi})^2$. It is worth noting, by comparing Eqs. (7) to (1), that the

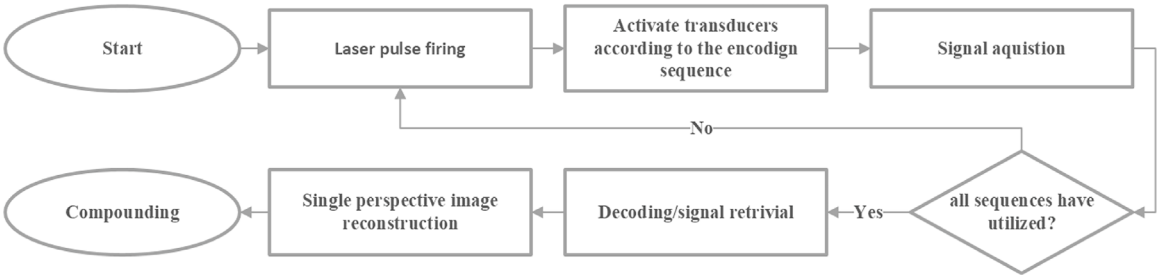

Fig. 1. The flowchart of the proposed imaging method. In each imaging session, multiple apertures are active simultaneously with respect to an encoded sequence and superimposed signals are recorded. The signals are then decoded before reconstructing and compounding the final image.

same amount of gain g can be seen for single perspective images when MAES is applied over conventional PAI, i.e.,

$$\mathrm{SNR}_{\mathrm{st}} = g\,\mathrm{SNR}_{\mathrm{conv}} \tag{10}$$

2.2. Encoding sequences

The choice of encoding sequence significantly impacts the final SNR of the MP-PAI system. In encoded multi-aperture imaging, the coding matrix $\mathbf{W}$ has to be orthogonal and invertible so that the decoding process can be obtained efficiently by applying $\mathbf{W}^{-1}$. Regarding Eq. (7), to maximize the $\mathrm{SNR}_{\mathrm{enc}}$ gain, we need to employ an encoding matrix whose inverse has the smallest possible entries. A good example of these multiplexing matrices are Hadamard matrices, which are of the order $M = 2^n$ for $n = 1, 2, 3, \ldots$ with bipolar elements, i.e, ± 1 [28]. The inverse version of the Hadamard matrix is just a scaled version of itself $\mathbf{H}^{-1} = \frac{1}{M}\mathbf{H}$, so the $\mathrm{SNR}_{\mathrm{enc}}$ gain compared to a conventional imaging scheme would be linearly increasing with a factor of M. For Hadamard encoding, all apertures are active in each imaging session, and the received signal from each transducer is either directly added or subtracted from the channel. Hadamard matrices are only available for 2^n orders, so they cannot be used for encoded imaging using any arbitrary numbers of transducers. In these cases, there may exist an encoding matrix with optimum properties [29].

A unipolar encoding technique (in which the elements are either 0 or 1), on the other hand, can be easily implemented. Such encoding sequences can be obtained by altering the bipolar matrices. For instance, by eliminating the first row and column of the Hadamard matrix and replacing the elements of 1s with 0s and elements of −1s with 1s. The resulting matrix is called the S-sequence matrix and is of the order $M = 2^n - 1$ for $n = 1, 2, 3, \ldots$ [23]. The entries in the inverse matrices are $2/(M+1)$ fold the entries in the S-sequence matrix. Hence, the $\mathrm{SNR}_{\mathrm{enc}}$ gain is expected to be $g = (M+1)^2/4M$ over conventional MP-PAI.

Now that we have established this theoretical framework, we evaluate the S-sequence encoding in both simulations and experiments. General bipolar encoding schemes, consisting of truncated versions of Hadamard matrices, are evaluated in simulations. To construct these matrices, we remove the first row and column resulting in a bipolar matrix of order $2^n - 1$ for $n = 1, 2, 3, \ldots$.

2.3. Simulations

In both the simulation study and the experimental study, the impact of aperture encoding is shown for the example of carotid plaque imaging, which is a major application of our previously proposed MP-PAI system [7]. For the numerical studies, a Monte–Carlo method is utilized to simulate the optical fluence in 2D. The Monte Carlo simulations are carried out using an in-house grid-based implementation that tracks photon packets according to the microscopic Beer–Lambert law method. The k-Wave toolbox for MATLAB is employed to simulate the 2D acoustic wave propagation in the tissue. For further details, readers are encouraged to refer to the works presented in [7,30]. The simulation workflow employed in this study is consistent with the methodologies outlined in these references.

Table 1
Medium properties [31–35].

Label	SOS (m/s)	Density (Kg/m^3)	Scattering (1/cm^{-1})	Absorption (1/cm^{-1})
Blood	1578	1050	50	20.02
Plaque	1535	1033	150	9.70
ICG	1530	1050	100	5.40
PVA	1550	1200	15	0.50
Water	1480	1000	1	0.0

The parameters for the apertures used are aligned with the CMUTs utilized in the experiments (see Section 2.4). The medium is defined to be 70 mm wide in both directions with a spatial grid spacing of 4.7×10^{-5} m (Fig. 2(a)). It contains a vascular phantom with three micro-channels containing different constituents. The different medium properties are provided in Table 1 [31–35].

To simulate and compare conventional MP-PAI to MAES imaging, the coding matrix $\mathbf{W}$ is set to the identity matrix and an encoding matrix, respectively. To mimic the thermal noise present in the experimental results, Gaussian noise is added to the channels. The k-Wave simulations are run with the standard Courant–Friedrichs–Lewy (CFL) number of 0.3, resulting in time steps of 9.6 ns. The data are then resampled to 32.25 MHz and processed using a band-pass with cut-off frequencies of 2.5 MHZ and 8.5 MHZ.

The transducers are positioned on one side of the medium at a fixed distance from the center. The simulations are acquired for various numbers of transducers ($M = 3$, 7 and 15) and while using different encoding sequences, namely, S-sequence and truncated Hadamard matrices. All transducers are distributed with equidistant angles within the range $[-\theta, \theta]$ where θ is the maximum angle from the center of the medium (see Fig. 2(a)). For 3 transducers, the maximum angle is 45°, and it is 90° for both 7 and 15 transducers configurations.

For statistical analysis, each simulation is run 10 times with the mentioned settings, and each run is performed with a new Monte–Carlo simulation and a new seed for the channel noise. The regions shown in Fig. 4(a) are used for SNR evaluations through Eq. (11).

To assess the performance of the MAES method under various channel SNRs, another set of simulations is conducted with settings similar to those using three transducers. In these simulations, the noise level is uniformly adjusted across all channels using a single magnitude factor for each simulation. This leads to different overall SNR values for each simulation, ranging from −4 dB in the first to 2.7 dB in the last. The RF channel SNR for each simulation is computed by manually segmenting the target and background regions within the simulated RF signals. The resulting compounded reconstructions for different imaging methods are evaluated in terms of SNR with regions shown in Fig. 4(a). Considering Eq. (9), the SNR gain g for MAES is multiplied to conventional MP-PAI results, i.e., evaluated image SNR, to have an expected gain in SNR for each simulation with a specific channel SNR.

2.4. Experiments

The imaging setup is composed of three CMUT prototypes (CM12; Philips, Netherlands) on a flexible substrate sharing the communication

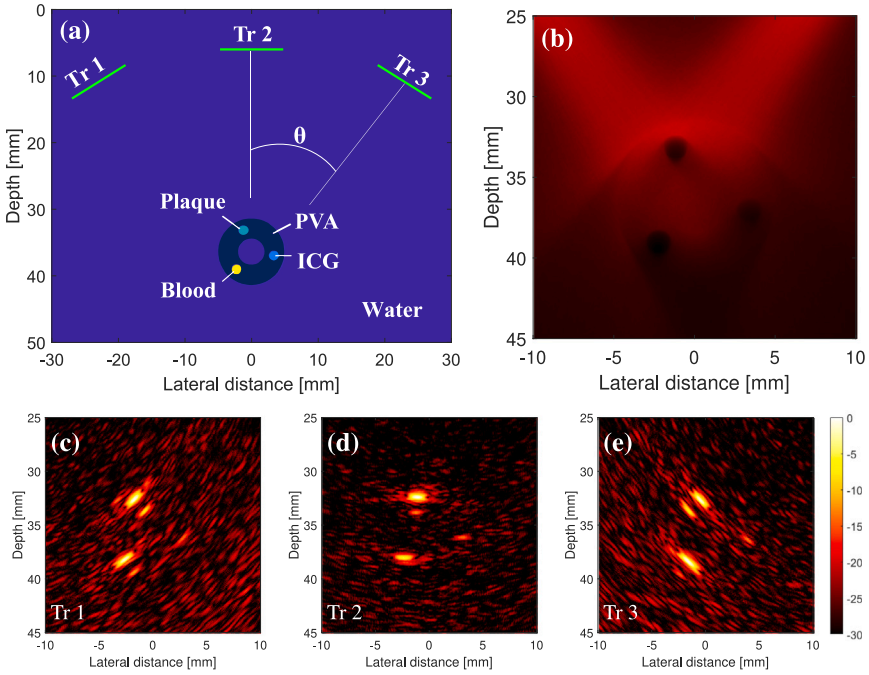

Fig. 2. The simulation medium depicts a three-transducers configuration (labeled Tr1, Tr2, and Tr3) and a phantom with four different components, each having a specific speed of sound, density, absorption and scattering coefficient described in Table 1 (a). The simulated fluence with the Monte Carlo approach (b), reconstructed images using transducers 1–3 plotted in log-scale with 30 dB dynamic range (c, d, and e).

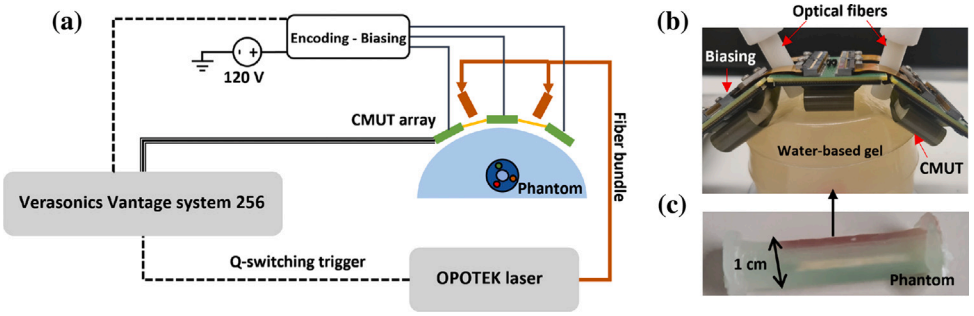

Fig. 3. The schematic of the setup (a) and the prototype CMUTs array placed on a neck mimicking water-based gel phantom (b); the plaque mimicking phantom which is embedded in the water-based gel phantom (c).

channels as proposed in [7] for human carotid plaque imaging (see Figs. 3(a, b)). The switching is performed by controlling the bias voltage of individual CMUTs. Each CMUT has 96 active elements with a center frequency of 7 MHz and a pitch of 102 μm. An OPOTEK RADIANT 355 tunable pulse laser is utilized to generate pulses at 545 nm, and a bifurcated fiber optic cable is employed to divide the light and deliver it to the phantom. The fluence out of fiber bundle is measured to be 6.8 mJ/cm^2 at 545 nm. During the imaging procedure, the raw radio frequency (RF) data are recorded and sampled at a 32 MHz sampling frequency. The orientation of each CMUT is obtained during the signal acquisition using a designated orientation sensor (9-axis MPU-6050 sensor, TDK InvenSense) [7]. A Verasonics Vantage 256 system is used to communicate with the CMUTs and the orientation sensors, as well as to control the Q-switch trigger of the laser and the biasing voltages of the CMUTs.

Since the prototype is not shielded well against electrical disturbance interference, the RF signals can be degraded with several strong, short pulses that appear simultaneously across the transducer elements. To remove these unwanted signals, a moving averaging window with a length of 50 is employed over the elements of the transducer, and the calculated average is subtracted from the RF data. Moreover, the previously mentioned band-pass filter (with the lower and higher cut-off frequencies of (2.5 MHz–8.5 MHz) is applied. The signals from each CMUT are reconstructed with respect to the position and orientation of the CMUTs on a grid with quarter of a lambda spatial spacing. Finally, the signals are compounded to form the final MP-PAI images.

A polyvinyl alcohol (PVA) plaque mimicking phantom with a diameter of 1 cm is prepared as described in [7]. The 2 mm inclusions were filled with porcine blood, indocyanine green in water solution 0.1 mg/ml (ICG), and plaque tissue (see Fig. 3(c)). The blood was prepared with 1% (weight/volume) EDTA to prevent coagulation. The plaque tissue was removed from the outer layer of an endarterectomy plaque that was obtained from the Catharina Hospital in Eindhoven. The patient has given informed consent to participate in this study. In experiments, the PVA phantom was placed around 3.5 cm deep from the surface of the CMUTs using stacks of gel pads (Aquaflex gel, Parker Laboratories) (Fig. 3(b)).

2.5. Data analysis and comparison

The MAES method is compared to conventional MP-PAI of [7] in terms of SNR. All images are formed using pixel-wise Delay-And-Sum (DAS) algorithm without any apodization by coherently compounding the single perspective reconstructions of CMUTs. No post-processing is applied on the reconstructed images. These images are assessed

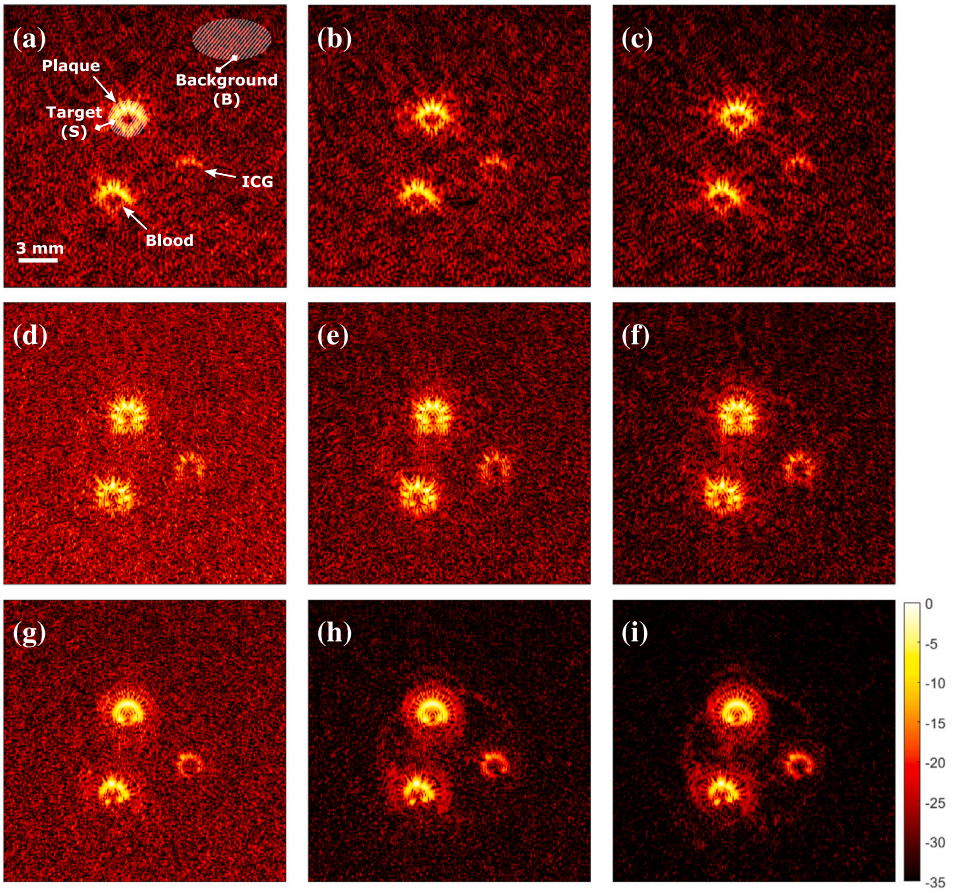

Fig. 4. Coherent compounding of simulation results for the imaging configuration based on three (a, b, c; top row), seven (d, e, f; middle row), and 15 (g, h, i; bottom row) transducers for respectively conventional transmission schemes (a, d, g; left column), S-sequence encoding (b, e, h; middle column), and truncated Hadamard encoding (c, f, i; right column) techniques; all images are plotted in log-scale with a dynamic range of 35 dB.

before log-compression (yet after envelope detection, without any normalization). To assess the SNR, two elliptic regions are chosen: the target region is chosen so that it covers one of the microchannels in the phantom, and the background region is selected to contain noise, i.e., it includes neither actual photoacoustic sources nor their sidelobe artifacts. The SNR metric is defined in decibels as follows:

$$\mathrm{SNR} = 10\log_{10}\frac{\mu_s}{\mu_b} \tag{11}$$

where $\mu_b = \mathbb{E}\{|B_i|^2\}$ and $\mu_s = \mathbb{E}\{|S_i|^2\}$ are the mean values of the envelop pressures squared in either the background (B) or the target regions (S).

3. Results

3.1. Simulation results

Fig. 4 shows the coherently compounded results of simulations using 3, 7, and 15 transducers for the conventional, S-sequence, and truncated Hadamard encoding techniques. The results of S-sequence, and especially truncated Hadamard encodings present a darker background (background noise suppression) with respect to conventional MP-PAI for the same number of transducers. This indicates an improvement of SNR when MAES is employed over conventional MP-PAI. By comparing the results for different numbers of transducers, it can be seen that adding more apertures leads to better suppression of background noise, especially when MEAS is used.

The statistical SNR evaluation results are summarized in Table 2 with reference to their corresponding configurations. The SNR for S-sequence and truncated Hadamard encodings with respect to conventional imaging increased by 1.2 and 2.5 dB for three transducers, 3.5 and 5.9 dB for seven transducers, and 5.8 and 8.8 dB for 15 transducers, respectively. The theoretical SNR gain for S-sequence and truncated Hadamard encodings over conventional imaging is expected to be respectively 1.2 and 3 dB for three apertures, 3.6 and 6 dB for seven apertures, and 6.3 and 9 dB for 15 apertures (see Eq. (9)). The deviation decreases for a higher number of transducers, as can be seen from Table 2 where the standard deviation for the triple-aperture setup is the highest and decreases subsequently for a higher number of CMUT transducers and transmit-receive events.

Table 2
Calculated SNR (in decibel) for the imaging results shown in Fig. 4.

Configuration	Conventional	S-sequence	Hadamard
3; Fig. 4 (a–c)	9.9 ± 0.4	11.1 ± 0.3	12.4 ± 0.4
7; Fig. 4 (d–f)	17.7 ± 0.2	21.2 ± 0.2	23.6 ± 0.2
15; Fig. 4 (g–i)	19.6 ± 0.2	25.4 ± 0.1	28.4 ± 0.1

Fig. 5 depicts the effect of different channel SNR on the final compounded results using the three-transducer setup. Three examples of compounded conventional MP-PAI images are provided in Figs. 5(a–c) where the channel SNR is −4, −0.1, and 2.7 dB, respectively. The SNR of the images is calculated using the same target and background regions defined in Fig. 4(a). The results are given in Fig. 5(d) along with the expected (theoretical, Eq. (9)) SNR gain for encoding methods. Regardless of SNR magnitude, the improvement over conventional MP-PAI is around 1.2 dB for the S-sequence, and 3 dB for the truncated Hadamard encoding methods, respectively. These findings are consistent with the theoretical expectations delineated earlier (see Eq. (9)).

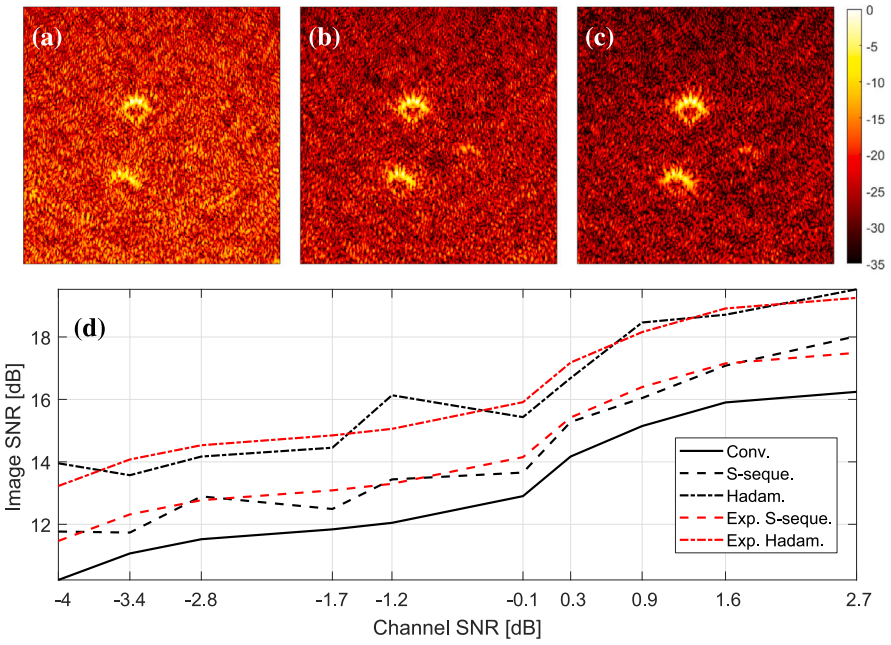

Fig. 5. Coherently compounded MP-PAI images using three transducers for channel SNR of −4, −0.1, and 2.7 dB (a–c), respectively; all images are plotted in log-scale with a dynamic range of 35 dB. SNR evaluations of the results for different methods (d), namely, conventional imaging (solid line), S-sequence (dashed line), and truncated Hadamard (dotted dashed line) encodings, with different channels SNR ranging from −4 to 2.7 dB; the analytical expectations are indicated with a dashed red line for S-sequence encoding and a dotted dashed red line for truncated Hadamard encoding.

3.2. Experimental results

The reconstructed single perspective images obtained with all three CMUTs and their coherently compounded results using conventional MP-PAI and S-sequence encoding are shown in Fig. 6. All the results are evaluated and the SNR values are provided at the bottom right of each image. The regions where the SNR is evaluated are indicated by two dashed elliptic regions for target and background noise (see Fig. 6(a)).

For the background region, the encoding method resulted in better noise suppression leading to improved contrast over the conventional MP-PAI results. By comparing results presented in Fig. 6, the gain in SNR of S-sequence encoding over conventional PAI are 2.3, 0.6, and 1.6 dB for the first, second, and third CMUT, respectively. The compounded S-sequence encoding result achieved a 1.5 dB improvement in SNR over the conventional method.

4. Discussion

In this work, a novel multi-aperture encoding scheme (MAES) is proposed to increase the SNR of a multi-perspective photoacoustic imaging (MP-PAI) system with multiple CMUTs and multiplexed shared RF channels. MAES was validated thoroughly in terms of SNR values for both simulations and experiments for both the unipolar and bipolar encoding sequences. Since all applied processes for MAES imaging exhibit linearity, we opt to evaluate the results using SNR rather than a more complex metric. All the results confirm the theory and demonstrate the potential of the multi-aperture encoding scheme to improve the SNR, especially for a large number of transducers. Please note that the purpose of this study is not focused on providing the optimal encoding sequences and one may find an encoding matrix with a specific order that outperforms S-sequence or truncated Hadamard encoding methods.

The results depicted in Fig. 4 and their statistical analysis, given in Table 2, in general match well with our theoretical expectation SNR gain over the conventional MP-PAI. However, in some cases, the SNR values deviated from the expected analytical approach. This can be caused by the fact that we assumed the noise to be perfectly independent for two separate sessions in theory, which is not always the case, even for simulations. With a finite set of samples, there is always some degree of correlation. In the results presented in Fig. 4, a circular artifact can be seen around the micro-channel especially for the cases where the noise is suppressed effectively, namely Figs. 4(h) and (g). The pressure waves originated from the boundary of a micro channel travel outward and inward relative to the vessel boundary. Inward waves, traveling inside the micro-channel, are reflected, and captured by transducers, creating circular shapes around the channel Hence, the artifact appears with twice the diameter of the micro-channels. This artifact is similar to reverberation artifacts in ultrasound imaging. Equally important, the compounding of the structures' sidelobes into the final image plays a critical role in the formation of artifacts around the micro-channels.

the S-sequence encoding outperformed the conventional MP-PAI in all individual perspectives as well as the coherent compounding result. However, the deviation of the experimental results from the analytically expected SNR gain (Eqs. (9) and (10)) is much higher than observed in the simulations. This could be explained by the presence of actual photoacoustic signals or their sidelobes in the region that is assumed to be only the noise. Besides, application of MAES method demands different electrical connections of CMUTs which can also affect the evaluated SNR. Still, by compounding the results, S-sequence encoding obtained a 1.5 dB improvement over the conventional method, which aligned well with theoretical expectation (see Eq. (9)).

The results consistently aligned with our theoretical expectations, demonstrating an improvement in contrast when MAES was employed, especially when using a large(r) number of transducers and truncated Hadamard encoding. It is worth noting that the proposed method was evaluated using stationary targets. Additionally, the multiplexing in time technique was still applied for imaging, which can decrease the overall imaging frame rate. A potential concern is that a spatial shift between two separate imaging sessions with shared transducers may lead to decorrelation of the signals which will in turn lead to sub-optimal decoding, decorrelation of structures, and appearance of ghosting artifacts. Nevertheless, these challenges can be mitigated using high frame rate imaging systems or motion correction algorithms, making the method viable for in vivo applications. Enhancing the system's speed

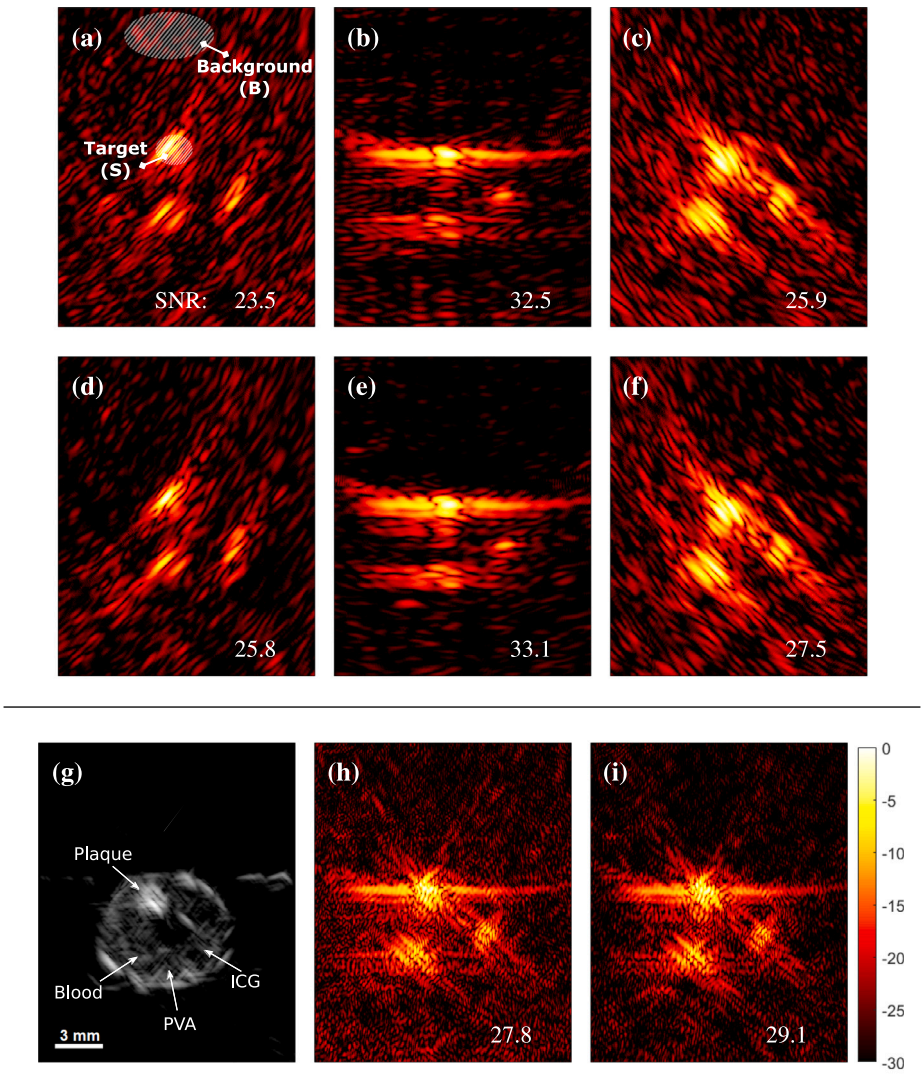

Fig. 6. Reconstructed single perspective photoacoustic images for each CMUT using conventional MP-PAI (a–c; top row) and S-sequence encoding scheme (d–f; middle row) as well as their coherently compounded result for conventional MP-PAI (h) and S-sequence encoding scheme (i), obtained in the carotid plaque phantom. The compounded ultrasound image is given in (g). The SNR value is provided at the bottom right side of each image. All photoacoustic images are plotted in log-scale with a dynamic range of 30 dB.

is feasible with faster light sources and advanced electronics (e.g. fast analog switches). Furthermore, exploring bipolar encoding techniques, such as Hadamard encodings, may offer additional opportunities to boost the SNR for the proposed MAES in both PAI and US imaging with multiple transducers.

5. Conclusion

In this paper, we developed a Multi-Aperture Encoding Scheme (MAES) to improve the SNR in Multi-Perspective Photoacoustic Imaging (MP-PAI) through the use of multiple spatially separated CMUTs. We proposed a model to calculate the expected gain for MAES using an arbitrary encoding sequence over conventional MP-PAI. Both simulations and experimental evaluations affirmed the theory, showcasing the potential of the MAES method.

Employing only three transducers in experiments, MAES achieved already an SNR gain of 1.5 dB for S-sequence encodings compared to conventional MP-PAI. Simulations demonstrated that the SNR gain over MP-PAI can be enhanced to about 9 dB when MAES was applied using a bipolar encoding sequence in a 15-transducer configuration. Moreover, it was shown that MAES SNR gain over MP-PAI remains independent of channel SNR.

MAES was evaluated in stationary phantoms. There is a need to explore the impact of the moving targets on the method and possibly increase the system's imaging frame rate. Future research will focus on utilizing analog inverters and switches, as well as deploying additional transducers, to facilitate the usage of binary sequences and extend the applicability of MAES to multi-perspective ultrasound imaging.

CRediT authorship contribution statement

Amir Gholampour: Writing – original draft, Software, Methodology, Investigation, Conceptualization. **Camilo Cano:** Software, Investigation. **Marc R.H.M. van Sambeek:** Writing – review & editing, Supervision, Resources. **Richard Lopata:** Writing – review & editing, Supervision, Resources. **Min Wu:** Writing – review & editing, Supervision, Resources. **Hans-Martin Schwab:** Writing – review & editing, Supervision, Investigation.

Declaration of competing interest

The authors declare the following financial interests/personal relationships which may be considered as potential competing interests: Marc R. H. M. van Sambeek, Min Wu reports financial support was

provided by Jaap Schouten Foundation. If there are other authors, they declare that they have no known competing financial interests or personal relationships that could have appeared to influence the work reported in this paper.

Data availability

Data will be made available on request.

References

[1] M. Mehrmohammadi, S. Joon Yoon, D. Yeager, S. Y. Emelianov, Photoacoustic imaging for cancer detection and staging, Curr. Mol. Imaging (Discontinued) 2 (1) (2013) 89–105.

[2] M. Xu, L.V. Wang, Photoacoustic imaging in biomedicine, Rev. Sci. Instrum. 77 (4) (2006) 041101.

[3] P. Beard, Biomedical photoacoustic imaging, Interface Focus 1 (4) (2011) 602–631.

[4] S. Jeon, J. Kim, D. Lee, J.W. Baik, C. Kim, Review on practical photoacoustic microscopy, Photoacoustics 15 (2019) 100141.

[5] R. Ellwood, O. Ogunlade, E. Zhang, P. Beard, B. Cox, Photoacoustic tomography using orthogonal Fabry–Pérot sensors, J. Biomed. Opt. 22 (4) (2016) 041009.

[6] X.L. Deán-Ben, E. Merčep, D. Razansky, Hybrid-array-based optoacoustic and ultrasound (OPUS) imaging of biological tissues, Appl. Phys. Lett. 110 (20) (2017) 203703.

[7] A. Gholampour, J.-W. Muller, C. Cano, M.R. van Sambeek, R. Lopata, H.-M. Schwab, M. Wu, Multiperspective photoacoustic imaging using spatially diverse CMUTs, IEEE Trans. Ultrason. Ferroelectr. Freq. Control 70 (1) (2022) 16–24.

[8] A. Caronti, G. Caliano, R. Carotenuto, A. Savoia, M. Pappalardo, E. Cianci, V. Foglietti, Capacitive micromachined ultrasonic transducer (CMUT) arrays for medical imaging, Microelectron. J. 37 (8) (2006) 770–777.

[9] K. Brenner, A.S. Ergun, K. Firouzi, M.F. Rasmussen, Q. Stedman, B.P. Khuri-Yakub, Advances in capacitive micromachined ultrasonic transducers, Micromachines 10 (2) (2019) 152.

[10] J. Joseph, B. Ma, B.T. Khuri-Yakub, Applications of capacitive micromachined ultrasonic transducers: A comprehensive review, IEEE Trans. Ultrason. Ferroelectr. Freq. Control 69 (2) (2022) 456–467, http://dx.doi.org/10.1109/TUFFC.2021.3112917.

[11] M. Vallet, F. Varray, J. Boutet, J.-M. Dinten, G. Caliano, A.S. Savoia, D. Vray, Quantitative comparison of PZT and CMUT probes for photoacoustic imaging: Experimental validation, Photoacoustics 8 (2017) 48–58.

[12] N.J. Petterson, M.R.H.M. van Sambeek, F.N. van de Vosse, R.G.P. Lopata, Enhancing lateral contrast using multi-perspective ultrasound imaging of abdominal aortas, Ultrasound Med. Biol. 47 (3) (2021) 535–545.

[13] H. De Hoop, N.J. Petterson, F.N. Van De Vosse, M.R.H.M. Van Sambeek, H.-M. Schwab, R.G.P. Lopata, Multiperspective ultrasound strain imaging of the abdominal aorta, IEEE Trans. Med. Imaging 39 (11) (2020) 3714–3724.

[14] M. Erfanzadeh, Q. Zhu, Photoacoustic imaging with low-cost sources; A review, Photoacoustics 14 (2019) 1–11.

[15] T.X. Misaridis, J.A. Jensen, Space–time encoding for high frame rate ultrasound imaging, Ultrasonics 40 (1–8) (2002) 593–597.

[16] P. Gong, P. Song, S. Chen, Ultrafast synthetic transmit aperture imaging using Hadamard-encoded virtual sources with overlapping sub-apertures, IEEE Trans. Med. Imaging 36 (6) (2017) 1372–1381.

[17] C. Ceroici, K. Latham, R. Chee, B. Greenlay, Q. Barber, J.A. Brown, R. Zemp, 3D photoacoustic imaging using Hadamard-bias encoding with a crossed electrode relaxor array, Opt. Lett. 43 (14) (2018) 3425–3428.

[18] T. Harrison, A. Sampaleanu, R.J. Zemp, S-sequence spatially-encoded synthetic aperture ultrasound imaging [correspondence], IEEE Trans. Ultrason. Ferroelectr. Freq. Control 61 (5) (2014) 886–890.

[19] H.K. Zhang, K. Kondo, M. Yamakawa, T. Shiina, Coded excitation using periodic and unipolar M-sequences for photoacoustic imaging and flow measurement, Opt. Express 24 (1) (2016) 17–29.

[20] E. Hahamovich, A. Rosenthal, Ultrasound detection arrays via coded Hadamard apertures, IEEE Trans. Ultrason. Ferroelectr. Freq. Control 67 (10) (2020) 2095–2102.

[21] R.J. Zemp, A. Sampaleanu, T. Harrison, S-sequence encoded synthetic aperture B-scan ultrasound imaging, in: 2013 IEEE International Ultrasonics Symposium, IUS, IEEE, 2013, pp. 593–595.

[22] S. Nikolov, J.A. Jensen, Comparison between different encoding schemes for synthetic aperture imaging, in: Medical Imaging 2002: Ultrasonic Imaging and Signal Processing, vol. 4687, SPIE, 2002, pp. 1–12.

[23] Q.M. Barber, R.J. Zemp, Photoacoustic–ultrasound tomography with S-sequence aperture encoding, IEEE Trans. Ultrason. Ferroelectr. Freq. Control 64 (4) (2017) 688–693.

[24] E. Hahamovich, S. Monin, Y. Hazan, M. Nagli, A. Rosenthal, 3D optoacoustic tomography via coded acoustic apertures, in: Photons Plus Ultrasound: Imaging and Sensing 2021, vol. 11642, International Society for Optics and Photonics, 2021, p. 116420D.

[25] M.F. Beckmann, H.-M. Schwab, G. Schmitz, Optimized SNR simultaneous multispectral photoacoustic imaging with laser diodes, Opt. Express 23 (2) (2015) 1816–1828.

[26] S.A. Telenkov, R. Alwi, A. Mandelis, Photoacoustic correlation signal-to-noise ratio enhancement by coherent averaging and optical waveform optimization, Rev. Sci. Instrum. 84 (10) (2013).

[27] J.-W. Muller, R. van Hees, M. van Sambeek, P. Boutouyrie, M. Rutten, P. Brands, M. Wu, R. Lopata, Towards in vivo photoacoustic imaging of vulnerable plaques in the carotid artery, Biomed. Opt. Express 12 (7) (2021) 4207–4218.

[28] K.J. Horadam, Hadamard Matrices and Their Applications, Princeton University Press, 2006, pp. 9–11.

[29] T. Banica, I. Nechita, K. Życzkowski, Almost Hadamard matrices: General theory and examples, Open Syst. Inf. Dyn. 19 (04) (2012) 1250024.

[30] J.-W. Muller, M.Ü. Arabul, H.-M. Schwab, M.C.M. Rutten, M.R.H.M. van Sambeek, M. Wu, R.G.P. Lopata, Modeling toolchain for realistic simulation of photoacoustic data acquisition, J. Biomed. Opt. 27 (9) (2022) 096005, http://dx.doi.org/10.1117/1.JBO.27.9.096005.

[31] IT'IS Foundation, Tissue properties database, 2022, https://itis.swiss/virtual-population/tissue-properties/database/.

[32] S.L. Jacques, Optical properties of biological tissues: A review, Phys. Med. Biol. 58 (11) (2013) R37.

[33] S. Jacques, P. Scott, OMLC spectera database, 2018, https://omlc.org/spectra/.

[34] M.U. Arabul, M. Rutten, F. van de Vosse, R. Lopata, Optical and acoustic characterization of freeze-thawed polyvinyl alcohol gels, in: 2014 IEEE International Ultrasonics Symposium, IEEE, 2014, pp. 2410–2413.

[35] M.L. Landsman, G. Kwant, G.A. Mook, W.G. Zijlstra, Light-absorbing properties, stability, and spectral stabilization of indocyanine green, J. Appl. Physiol. 40 (4) (1976) 575–583.

Amir Gholampour received the master's degree in biomedical engineering from Babol university of technology, Babol, Iran, in 2018. He is a Ph.D. candidate in the Photoacoustics and Ultrasound Laboratory Eindhoven (PULS/e lab) at Eindhoven University of Technology, his research focuses on ultrasound and photoacoustic imaging, beamforming, and signal processing.

Camilo Cano received his master's degree in applied physics in 2018 from EAFIT University, Medellin, Colombia. In 2020 joined the Photoacoustics and Ultrasound Laboratory at Eindhoven University of Technology as a Ph.D. student.

Marc R.H.M. van Sambeek earned his medical degree from Catholic University, Nijmegen, The Netherlands, in 1986, and his Ph.D. from Erasmus University, Rotterdam, The Netherlands, in 1998, specializing in intravascular ultrasound and peripheral.

Richard G.P. Lopata received the M.Sc. degree in biomedical engineering from the Eindhoven University of Technology (TU/e), Eindhoven, The Netherlands, in 2004, and the Ph.D. degree from Radboudumc, Nijmegen, He has been an Associate Professor at TU/e, heading the Photoacoustics and Ultrasound Laboratory Eindhoven (PULS/e lab) since 2014. The PULS/e lab facilitates research on technology development in the areas of ultrasound functional imaging, photoacoustics, and image-based modeling aimed to facilitate in and/or improve clinical decision making for cardiovascular, musculoskeletal, and abdominal applications.

Min Wu is an assistant professor in PULS/e LAB in TU/e. She received her Ph.D. degree in intravascular photoacoustic imaging of vulnerable plaques in Erasmus MC, in 2017 and then continue working on photoacoustic imaging as a post-doc in TU/e. Her current research includes, (spectroscopic) photoacoustic imaging on carotid plaques and osteoarthritis, photoacoustic imaging system design and optimization, and tissue composition characterization.

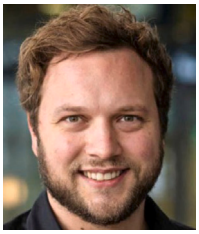

Hans-Martin Schwab received the master's and Ph.D. degrees in electrical engineering from Ruhr University Bochum, Bochum, Germany, in 2013 and 2018, respectively. He is currently an Assistant Professor with the Laboratory for Ultrasound and Photoacoustics (PULS/e), Eindhoven University of Technology, Eindhoven, The Netherlands, working on novel approaches for ultrasound acquisition and model-based image reconstruction.